The heating mechanism of electrons in the shock front of an expanding plasma

Plasma Sources Sci. Technol. 3 (1994) 511–520. Printed in the UK

The heating mechanism of electrons in the shock front of an expanding plasma

M C M van de Sanden, R van den Bercken and D C Schram

Department of Physics, University of Technology Eindhoven, PO Box 513, 5600 MB Eindhoven, The Netherlands

Received 11 February 1993, in final form 24 May 1994

Abstract. The heating of the electron gas in the shock front of an expanding plasma jet is modelled. In the expansion, due to the large pressure gradient, a current is generated which, besides the heating by three-particle recombination, takes care of additional heating of the electron gas. It is shown, by means of a quasi one-dimensional model in combination with a two-dimensional calculation of the electrical properties, that the preheating of the electron gas in front of the shock can be explained by Ohmic dissipation of the generated current density in combination with the electron heat conduction. The outcome of the model is compared with experimental results.

1. Introduction

Electrons play an important role in a plasma. Usually they are responsible for the excitation, ionization and dissociation of the different species. Because they have a small mass they play a dominant role in maintaining the electrical field within a plasma. In this paper we will discuss the heating mechanism of the electron gas in the stationary shock front of the plasma expanding from a cascaded arc. These types of plasma are used in the recently developed fast deposition method (up to a factor of hundred higher rates than with the conventional deposition methods) for several types of carbon coatings (ranging from crystalline graphite and diamond to amorphous hydrogenated carbon, the so called 'diamond like coatings') and amorphous hydrogenated silicon layers [1–3]. Also the use of these type of plasmas for bright atomic and ionic hydrogen sources is presently under investigation [4]. Furthermore, these types of plasmas are used in thrusters for space applications [5].

A preceding paper was devoted to the behaviour of heavy particles both in the supersonic expansion and in the shock front occurring in these types of plasmas [6]. It was found that the heavy particles, both ions and neutral particles, expand adiabatically—similar to the process in an ideal gas. The motion of the ions is decoupled from the neutral particles in the stationary shock, where the neutral particles still behave adiabatically. Instead, the motion of the ions is influenced by the electrons due to the electrical field.

The heating mechanism of the electron gas in a supersonic expansion was treated in a separate paper [7] where it was shown that the main heat source of the electrons occurs by means of three-particle recombination. This paper aims to conclude the picture of the expanding plasma jet in argon as it deals with the motion of the electron gas in the stationary shock front. The main subject is to explain the preheating of the electron gas, as was established experimentally in [6]. A model of the expanding plasma jet will be developed and compared with experimental results.

2. Experiment

As discussed in a previous paper, the measurements of electron density and temperature and the neutral particle density are performed on an argon plasma expanding from a cascaded arc [6]. Here we will focus mainly on the measurement with the settings as given in table 1. For more details the reader is referred to the original paper [6]. The main issue we want to address in this paper is shown in figure 1, where n_e and T_e on the axis of the plasma jet are shown as a function of the distance from the exit of the cascaded arc. As can be seen, the electron temperature jumps ahead of the increase in the electron density. The increase in electron density is

Table 1. The setting of the cascaded arc set-up. For explanation see text.

I_{arc}	45 A
V_{arc}	160 V
Ar flow	58 sccs^{-1}
p	40 Pa

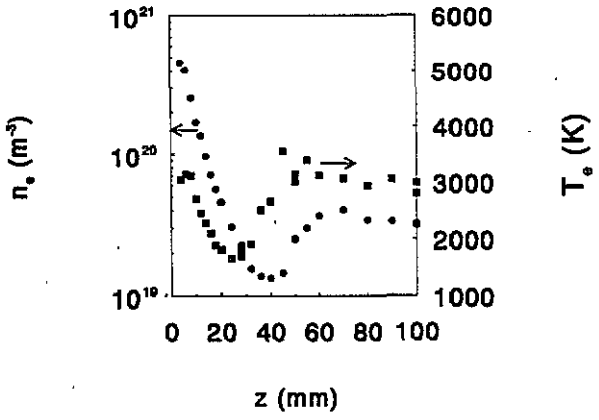

Figure 1. The difference between the electron density and electron temperature jump for setting 1 of table 1.

caused by the gas–dynamic shock transition of the ions which forces the electrons to compress due to the strong electric field generated [6]. This observation is noted for all the settings measured up to now, i.e. different flow and/or current in the cascaded arc or a different background pressure. Furthermore, the difference in the positions of the electron temperature and the electron density jump was also measured by Fraser *et al* [8], Kirchhoff and Talbot [9], Jenkins [10] and Poissant and Dudeck [11] using a Langmuir probe diagnostic. All these measurements were performed on a similar expanding plasma in argon (e.g. background pressures, flow, etc), as is considered in this work. The result obtained by Christiansen [12], using a Langmuir probe diagnostic in a caesium seeded argon plasma, shows also preheating of the electron gas in front of the electron density jump. Bogen *et al* [13] and McNeill [14] used Thomson scattering to determine the electron density and temperature in a deuterium shock tube experiment. In both cases the electrons are preheated upstream of the ion density shock. We therefore assume that preheating of the electron gas in front of the shock in these types of plasma is of a more general nature.

3. Model

In this section the observed preheating of the electron gas (see figure 1) will be analysed in more detail using a quasi one-dimensional model. The model presented will include the temperature non-equilibrium between the heavy particles (neutral particles and ions) and the electrons. Furthermore, the current density generated in the expansion by the strong pressure force is included. As discussed, an important feature is the fact that the electrons, due to their small mass, do not undergo a gas–dynamical shock transition. That is, the energy required to compress the electrons in the ion shock front does not originate from the directed kinetic energy of the electrons in the expansion, since this kinetic energy is negligible compared with the thermal energy of the electrons. Instead, this energy is delivered by the generated electric field of the electron–ion fluid and partially by the temperature non-equilibrium [6, 15]. In an adiabatic shock transition of the electrons, T_e would increase as $n_e^{2/3}$. However, in the region of the ion shock front the heat sources in the electron energy balance, e.g. Ohmic dissipation and electron heat conduction, are important and lead to a more complicated situation.

The usual explanation for preheating of the electron gas given in the literature is that, because the electron heat conduction is large, electron thermal energy leaks back to positions ahead of the shock front, leading to local heating of the electron gas [15–17]. However, in this explanation the influence of the presence of a current density, which is generated in the expansion due to the strong electronic pressure force, is neglected. Heating due to this current density by Ohmic dissipation ahead of the density shock front is therefore possible. Later in this section, it will be shown that Ohmic dissipation, together with electron heat conduction, are the main causes for the preheating of the electron gas. The presence of a current density and the electron heat conduction results in a broad region of a monotonic increase of the electron temperature through the shock front.

Another possible mechanism for preheating of the electron gas is the mechanism of radiation absorption [18, 19]. In the present analysis this mechanism can be neglected since the shock strengths in this type of plasma are usually small and the observed temperatures and densities are lower [6].

To derive the equations for the quasi one-dimensional model, we start with the conservation equation for a current carrying two-temperature plasma [20, 21]. The electron mass balance is equal to

$$\nabla\cdot(n_e w_e) = -K_{rec,3} n_e^3 \tag{1}$$

where we have neglected two-particle recombination, which is much smaller than three-particle recombination [22]. Furthermore, the ionization is not taken into account because of the low electron temperature [6, 7]. $K_{rec,3}$ is the three-particle recombination coefficient and follows from the analysis of the electron gas in the expansion [6, 7]. For the heavy particles the mass balance is defined through

$$\nabla\cdot(n_h w_h) = 0 \tag{2}$$

where n_h and w_h are the heavy particle density and velocity respectively given by

$$n_h = n_0 + n_i \tag{3}$$

$$w_h = \frac{n_0 w_0 + n_i w_i}{n_0 + n_i} = (1-\alpha) w_0 + \alpha w_i \tag{4}$$

with α, the ionization degree, given by

$$\alpha = \frac{n_i}{n_0 + n_i}. \tag{5}$$

Since the inertia term in the electron momentum balance is proportional to the electron mass, this term is very

small compared to the pressure and friction terms in the electron momentum balance. Therefore the inertia term in the electron momentum balance is neglected. If the terms containing the electron viscosity (of the order $(\lambda_{ee}/L)^2 \ll 1$, where λ_{ee} is the mean free path for electron–electron collisions and L is a typical gradient length for the electron gas) and the momentum exchange with the neutral particles are omitted (of the order $\tau_{ei}/\tau_{e0} \ll 1$ where τ_{ei} and τ_{e0} are the collision times for electron–ion and electron–neutral interactions), the electron momentum balance is equal to (no magnetic field, $\boldsymbol{B} = 0$)

$$\nabla p_e + en_e\boldsymbol{E} = \boldsymbol{R}^{ei} \tag{6}$$

where $\boldsymbol{E}$ is the electrical field. The momentum exchange from the electrons to the ions is reflected in $\boldsymbol{R}^{ei}$, which is given by

$$\boldsymbol{R}^{ei} = en_e\eta\boldsymbol{j} - \gamma_0 n_e\nabla(k_b T_e) \tag{7}$$

where η is given by

$$\eta = \frac{\alpha_0 m_e}{n_e e^2 \tau_{ei}} \tag{8}$$

and the current density by

$$\boldsymbol{j} = en_e(w_i - w_e). \tag{9}$$

In equation (8) α_0, equal to 0.51, is a coefficient calculated by Braginskii [23]. The first term on the right-hand side of equation (7) is due to the difference in drift velocity between electrons and ions. The second term is the momentum exchange with the ions, because the collision rate is temperature dependent. The coefficient γ_0, equal to 0.71, is also calculated by Braginskii [23].

The heavy particle momentum balance, in the same approximation as equation (6), is given by

$$n_h m_h(w_h \cdot \nabla)w_h + \nabla p_h - en_e\boldsymbol{E} = -\boldsymbol{R}^{ei} \tag{10}$$

where p_h, the heavy particle pressure is given by $p_h = n_h k_b T_h$ and T_h is equal to

$$T_h = \frac{n_0 T_0 + n_i T_i}{n_0 + n_i} = (1-\alpha)T_0 + \alpha T_i. \tag{11}$$

In equation (10) we have neglected the viscosity term. Adding equations (6) and (10), the plasma momentum balance results

$$n_h m_h(w_h \cdot \nabla)w_h + \nabla p = 0 \tag{12}$$

with $p = p_e + p_h$ the total pressure. The equation is the equivalent of the Navier–Stokes equation in fluid mechanics [24]. If the magnetic field is included, a $\boldsymbol{j} \times \boldsymbol{B}$ term appears on the right-hand side [25] of the equation. This force is related to the rotation of the plasma [25] in the presence of a magnetic field.

The electron energy equation is given by

$$\nabla\cdot(n_e k_b T_e w_e) + n_e k_b T_e \nabla\cdot w_e + \nabla\cdot q_e = Q_e. \tag{13}$$

The heat source Q_e for the electron gas consists of Ohmic heating, heating by three-particle recombination, cooling by elastic collisions with the heavy particles and cooling by radiation processes such as two-particle recombination, the escape of line radiation and Brehmsstrahlung emission [26]. For the heat flux q_e the following form is assumed

$$q_e = -\kappa_e \nabla(k_b T_e) \tag{14}$$

where κ_e is the electron heat conductivity. The energy equation of the heavy particles is equal to

$$\nabla\cdot(n_h k_b T_h w_h) + n_h k_b T_h \nabla\cdot w_h + \nabla\cdot q_h = Q_h \tag{15}$$

where Q_h is the heat exchange between the electrons and heavy particles. A similar shape for heavy particle flux q_h is assumed as in equation (14) [27].

The effect of temperature non-equilibrium and current generation on the flow properties is best demonstrated by rewriting the balance equations (1), (2), (6), (12), (13) and (15) for a quasi one-dimensional situation [22]. This is done by expressing the electron drift velocity in the heavy particle velocity and the current density (equation (9)) neglecting the small difference between w_i and w_h (usually α is small), and using the fact that

$$\nabla\cdot j = 0. \tag{16}$$

The electron momentum balance, equation (6), is used to express the gradient of the electron temperature in the electric field, in the current density and in the gradient of the electron density. Furthermore, if all viscosity effects are neglected the final equations read

$$\frac{\partial\alpha}{\partial\xi} = -\frac{\alpha}{w_h} K_{rec,3} n_e^2 \tag{17}$$

$$\frac{\partial\rho}{\partial\xi} = \frac{\rho M_p^2}{(1-M_p^2-\zeta)}\frac{1}{A}\frac{\partial A}{\partial\xi} - \frac{2(Q_i^* + Q_j)}{5w_h R T_p(1-M_p^2-\zeta)} \tag{18}$$

$$\frac{\partial w_h}{\partial\xi} = \frac{w_h(1-\zeta)}{(1-M_p^2-\zeta)}\frac{1}{A}\frac{\partial A}{\partial\xi} + \frac{2(Q_i^* + Q_j)}{5w_h R T_p(1-M_p^2-\zeta)} \tag{19}$$

$$\frac{\partial T_e}{\partial\xi} = \frac{2T_e M_p^2}{3(1-M_p^2-\zeta)}\frac{1}{A}\frac{\partial A}{\partial\xi} + \frac{2(Q_e^* + Q_j + Q_\rho)}{3\alpha\rho w_h R} - \frac{T_e}{\alpha}\frac{\partial\alpha}{\partial\xi} - \frac{4T_e(Q_i^* + Q_j)}{15\rho w_h R T_p(1-M_p^2-\zeta)} \tag{20}$$

$$\frac{\partial T_h}{\partial\xi} = \frac{2T_h M_p^2}{3(1-M_p^2-\zeta)}\frac{1}{A}\frac{\partial A}{\partial\xi} + \frac{2Q_h^*}{3\rho w_h R} - \frac{4T_h(Q_i^* + Q_j)}{15\rho w_h R T_p(1-M_p^2-\zeta)}. \tag{21}$$

In equations (17)–(21), ρ, T_p and M_p respectively refer to the mass density

$$\rho = m_h n_h = m_h(n_0 + n_i) \tag{22}$$

the plasma temperature

$$T_p = T_h + \alpha T_e \tag{23}$$

and the plasma Mach number

$$M_p = \frac{w_h}{\sqrt{\frac{5}{3}RT_p}}. \tag{24}$$

The asterisk refers to the energy source term including the heat conduction term. $Q_t^* = Q_e^* + Q_h^*$ is the total heat source. The loss of energy due to line and free-free emission are neglected in Q_e^*, since these losses are much smaller than the other heat losses in the electron energy balance [22]. Q_j, Q_p, and ζ are given by

$$Q_j = \eta j_A^2\left(\frac{3}{2(\gamma_0+1)}+1\right) - j_A E_A \frac{3}{2(\gamma_0+1)} - \frac{k_b T_e j_A}{e\alpha}\frac{\partial\alpha}{\partial\xi} \tag{25}$$

$$Q_p = -\left(\frac{3}{2(\gamma_0+1)}+1\right)\frac{\alpha k_b T_e j_A}{e\rho}\frac{\partial\rho}{\partial\xi} \tag{26}$$

$$\zeta = -\frac{2}{5}\left(\frac{3}{2(\gamma_0+1)}+1\right)\frac{\alpha T_e}{T_p}\left(1-\frac{w_e}{w_h}\right). \tag{27}$$

In equations (25)–(27), j_A and E_A are the current density and the electrical field in the quasi one-dimensional approach respectively. The coordinate ξ in equations (17)–(21) refers to either the radius r of the source expansion models [28–30], or to the axial coordinate z, if the quasi one-dimensional approach [21] is considered. In the spherically symmetric case of the source expansion [28–30],

$$\frac{1}{A}\frac{\partial A}{\partial\xi} = \frac{2}{r} \tag{28}$$

and in the quasi one-dimensional case [21]

$$\frac{1}{A}\frac{\partial A}{\partial\xi} = \frac{2\tan(\phi)}{r_0 + z\tan(\phi)} \tag{29}$$

where ϕ is half of the angle of expansion. A is equal to r^2 in the source model and corresponds to the surface over which the plasma parameters are averaged in the quasi one-dimensional model. It is seen that the source model is equivalent to the quasi one-dimensional model for $z\tan(\phi) \gg r_0$ where r_0 is the radius of the plasma for $z = 0$. The quasi one-dimensional model is only valid if the axial gradients are much larger than the radial gradients. In the quasi one-dimensional model the parameters α, ρ, w_h, T_e, T_h, E_A and j_A refer to some surface averaged value [21,22,31]. In the source expansion case the parameters refer to the radial values of these parameters.

Equations (17)–(27) contain seven unknown parameters. Therefore, two additional equations are needed. These equations are the electron momentum balance (equation (6)) and the Maxwell equations

$$\nabla\cdot\boldsymbol{B} = 0 \tag{30}$$

$$\nabla\times\boldsymbol{B} = \mu_0\left(\boldsymbol{j} + \varepsilon_0\frac{\partial\boldsymbol{E}}{\partial t}\right) \tag{31}$$

$$\nabla\cdot\boldsymbol{E} = \frac{\rho_{el}}{\varepsilon_0} \tag{32}$$

$$\nabla\times\boldsymbol{E} = -\frac{\partial\boldsymbol{B}}{\partial t}. \tag{33}$$

In equation (32) ρ_{el} is given by

$$\rho_{el} = e(n_i - n_e). \tag{34}$$

Note that (compare with equations (17)–(27)) in contrast to ordinary gas–dynamics [32], the sonic condition ($M_p = 1$) is not necessarily at the position where $\partial^2 A/\partial\xi^2 = 0$. Note furthermore that, since $\zeta > 0$, if a current density is present, the Mach number can be smaller than unity to get an expansion behaviour, i.e. densities and temperatures decrease during the expansion. The adiabatic situation is reconstructed from equations (17)–(27), by putting all the source terms and the current density to zero. Note that, since the second term on the right-hand side of equations (18) and (19) is of the order M_p^{-2}, the expansion of the heavy particles is not too different from the adiabatic expansion as discussed previously [6, 7].

The calculation of the electron temperature by equation (20) depends, in contrast to the heavy particle properties, very much on the source terms Q_e^*, Q_j and Q_ρ. The reason for this is that the expansion terms in the electron energy balance are less important than in the other equations. In this respect, it is important to mention the electron heat conduction which is included in Q_e^*. Because the thermal velocity of the electrons is $(m_h T_e/m_e T_h)^{1/2}$ larger than that of the heavy particles, the transport of electron thermal energy by heat conductivity is very important and should be included. In the quasi one-dimensional model, an averaged value of the electron heat conductivity is taken by assuming a certain radial profile. The electron heat conductivity in the axial direction is fully included. In the discussion of the shock front in the next section, the electron heat conduction plays, beside the current density and the electric field, an important role. The current and electric field generation are the last non-equilibrium features discussed in this section.

As can be seen from equations (17)–(27), the differences between a situation with and without a current density are reflected by the correction factor ζ and additional heat sources Q_j and Q_ρ. The presence of a current density in the plasma results in a heating of the electrons if the heating due to Ohmic dissipation is larger than the cooling caused by the expansion. This means that the sum of Q_j and Q_ρ has to be considered. If the term proportional to $(M_p)^{-2}$, which is small for $M_p \gg 1$, is neglected, and if $Q_j > Q_\rho$ then the presence of an additional current density leads to an additional heating of the electron gas. If, on the other hand, $Q_j < Q_\rho$, the electron temperature is lowered by the presence of a current density. The right-hand side of equations (25) and (26) reflects the effect of cooling due to the expansion of the electron gas. More indirectly, the heavy particle motion and temperature are influenced

through the terms in equations (17)–(27) containing j_A and E_A.

To solve equations (17)–(27), the current density and the electric field have to be known. If the electron density and temperature are known (for instance from measurements or from an iterative scheme using equations (17)–(27) starting with j_A and E_A equal to zero), the current density and electric field are calculated by solving the electron momentum balance in combination with Poisson's equation (equation (32)) and appropriate boundary conditions. Here the model developed by Gielen and co-workers [25, 33] is adopted. This scheme determines the electric field self-consistently by calculating the charge separation from the electron momentum balance and using the condition equation (16). Since the current generation in case of a free expanding plasma is partly of a convective nature, two-dimensional effects in the determination of the current density and the electric field are very important. Therefore equations (6) and (32) are solved for a cylinder symmetric expanding plasma. Rewriting equation (32) for the electric potential Φ with $\boldsymbol{E} = -\nabla\Phi$ gives

$$\Delta\Phi = -\frac{\rho_{el}}{\varepsilon_0} \tag{35}$$

where ρ_{el} is determined from the divergence of the electron momentum balance

$$\rho_{el} = \varepsilon_0 \nabla \cdot \left(\eta \boldsymbol{j} - \frac{\nabla p_e}{e n_e} - \frac{\gamma_0 k_b \nabla T_e}{e} \right). \tag{36}$$

Equation (35) is solved with given boundary conditions. From the determined electric potential the current density is determined from [33]

$$\boldsymbol{j} = -\frac{\nabla\Phi}{\eta} + \frac{\nabla p_e}{e n_e \eta} + \frac{\gamma_0 k_b \nabla T_e}{e\eta}. \tag{37}$$

Thus, if the electron density and temperature are known, the current density and the electric field can be determined self-consistently.

The numerical procedure is as follows. First of all, the current density and electric field are determined from the local measurement of the electron density and temperature in the supersonic expanding plasma jet (see [6]), using the numerical procedure as described previously [25, 33]. A two-dimensional computer code with grid generation is developed [22], which runs on an IBM RS workstation. The computer code determines the generated electric field $\boldsymbol{E}$ and the generated current density $\boldsymbol{j}$ self-consistently in a cylindrically symmetric situation, by solving the momentum equation (equation (6)) together with Poisson's law (equation (32)) and the condition equation (16). The determined axial components of $\boldsymbol{j}$ and $\boldsymbol{E}$ are included in solving equations (17)–(27). These equations are solved for given initial conditions for the source model (equation (28)) using a fifth-order Runge–Kutta integration procedure on an IBM RS workstation. The calculation in the expansion region is completed at the position of the shock front, determined either with help of a given position or calculated from a condition as in Young's work [34]. At this position, a Mott–Smith [35] shape of the shock front for both the ions and the neutral particles is assumed wih different shock thicknesses L_0 and L_i [36, 37] and different Mach numbers $M_{0,i}$ and M_i for both neutral and electron–ion gas [6]. In the shock front the electron energy equation is solved, using the electron densities and gradients following the Mott–Smith ion shock front shape [6]. The described procedure in the shock front is identical to the work of Grewal and Talbot [15]. After the shock front the calculation is stopped.

4. Results

The results from the computer code, which calculates the current density $\boldsymbol{j}$ and the electric field $\boldsymbol{E}$ in the expanding plasma on the basis of the measured profiles, are discussed first. The other computer code uses the calculated axial components of $\boldsymbol{j}$ and $\boldsymbol{E}$ to determine their influence on the plasma parameters in the expansion region. This is discussed later in this section. The basic features of the calculations of the electric properties and the plasma parameters are demonstrated on the basis of calculations for the settings given in table 1.

Gielen and co-workers [25, 33] determined the generated current density, electric and magnetic field from an assumed electron density and temperature profile for three types of expanding plasma: the unipolar arc, the cathode spot and a laser produced plasma. The unipolar arc is comparable to the present situation of a plasma expanding from a cascaded arc, since the generated density is pressure induced and the self-generated magnetic field is small. In the present analysis the self-generated magnetic field is therefore neglected.

In this paper the electron density and temperature fields are not assumed but taken from a fit of the axial profiles of the electron density and temperature. However, the radial profiles for n_e and T_e were not measured at all axial positions. Therefore it is assumed that the radial dependence can be approximated by Gaussian profiles. For the settings of table 1, the width of these profiles is estimated from the measurements of the radial profiles of n_e and T_e [6]. The assumption that the radial profiles can be represented by Gaussians is not totally justified, especially in the supersonic expansion region. However, since the current density is pressure induced and since the axial component of the gradients is larger than the radial component, it is assumed that the influence of the shape of the radial profiles on the final magnitude of the current density on the axis is small.

A complication compared to previous work [25, 33] is the fact that the electron temperature is not constant in the expansion so that an extra contribution to the charge separation due to the dependency of the resistivity on the electron temperature should be taken into

account. This extra charge separation ρ_{el}^{η} is given by

$$\rho_{el}^{\eta} = j \cdot \nabla \eta. \tag{38}$$

It can be shown [22] that strictly speaking the algorithm developed previously [25, 33] in this situation does not lead to a solution of the considered problem. However, if the charge separation due to the non-isothermal character of the problem is small compared to the other charge separation terms, i.e. if

$$\frac{\rho_{el}^{\eta}}{\rho_{el}} \ll 1 \tag{39}$$

where ρ_{el} is the charge separation given by equation (36) with η constant, the previous algorithm [25, 33] will still lead to a solution of the problem. In the numerical calculations the charge separation ρ_{el} was determined by assuming that η is constant. After the calculation of the electric properties, the condition equation (39) was checked and was always found to be satisfied.

The results for the parameters on the axis are shown in figure 2 for the first 100 mm. In figure 2(*a*) the current density j_z is given as a function of z. The current density close to the exit of the cascaded arc is large (-5×10^6 A m^{-2}). As a function of z, the current density decreases rapidly to values of the order of -2×10^3 A m^{-2} at $z \approx 20$ mm. Between the electron temperature jump ($z \approx 25$ mm) and the density shock front ($z = 40$ mm) (see figure 1) the current density increases slowly to -3×10^3 A m^{-2}. The current density changes sign in the neighborhood of the shock front. Behind the shock front the current density becomes small for large z. The total current leaving the cascaded arc at the exit is approximately equal to 20 A. This current, of course, has to end up somewhere. As in the situation of the unipolar arc, most of the current going into the vessel returns within 40 mm back to the anode plate of the cascaded arc. The return of the current is due to the negative charge density ahead of the shock front. Likewise, the current density downstream of the $j_z = 0$ point is assumed to be balanced by a current density vortex which is toroidal shaped, leading to the fact that the current density integrated over the plasma beam area equals zero. In figure 2(*b*) the velocity difference $w_{ez} - w_{iz}$ between the electrons and ions is shown as a function of z. As can be concluded, the velocity difference is always positive ahead of the shock front, which means that the electrons move faster than the ions, as expected. The velocity difference between the electrons and ions is maximum at the exit of the cascaded arc. A second maximum is found between the electron temperature jump and the density shock fronts. Behind the shock front the electrons move slower than the ions. This is explained by the shape of the potential Φ_{axis} in the expanding plasma which is shown in figure 2(*c*). The typical double-layer structure in the neighborhood of the shock front is clearly seen. The first increase of the potential is a consequence of the acceleration of the electrons due to the pressure force and the second increase is a consequence of the shock front. The presence of the electrons results in a more positive potential behind the shock front, leading to the smaller compression of the ions in the shock front. After the shock front the potential becomes constant, i.e. the electric field vanishes. In figure 2(*d*) the different terms in the electron momentum balance, expressed as an equivalent electric field, are compared with each other. As can be seen the pressure term $-\nabla p_e/en_e$ is the current driving force, i.e. the pressure term is always larger than the electric field and larger than the temperature term in the electron momentum balance. In the neighbourhood of the shock, the electric field is of the order of the pressure force and approximately equal to 25 V m^{-1}. This is a much smaller electric field than that calculated by Greenberg *et al* [38] who calculated an electric field of 10^6 V m^{-1} in the shock front. The reason for this discrepancy is the fact that Greenberg *et al* [38] did not consider a shock front broadened by viscosity. This leads to a much smaller shock front thickness than in reality and related to this a much larger electric field.

To conclude, a significant velocity difference is found between the electron and the ions — it changes sign in the neighbourhood of the ion shock front. Furthermore, the double-layer shape of the electric potential was found, in agreement with the results for the shock front of the ions, where it was stated that the presence of electrons leads to a smaller compression of ions [6].

Now we will discuss the results of the model calculations using equations (17)–(27). Note that the calculation is not totally self-consistent since measurements are used to determine the current density and electric field. To start the Runga-Kutta integration the values of the plasma parameters have to be known at the exit of the cascaded arc. These values can either be taken from calculations of the parameters in the cascaded arc or deduced from measurements. The initial conditions are related to each other by the sonic condition. A problem is that equations (17)–(21) are singular for $M_p = 1$ if $\mathbf{j} = 0$. To avoid this singular behaviour the Mach number is usually chosen to be slightly higher than one at the sonic orifice [10, 29]. If $\mathbf{j} \neq 0$ the problem is similar. Another way is to start the calculation at a position different from the sonic orifice. Here the last method is used.

As discussed, the expansion of the heavy particles is almost identical to the adiabatic expansion of a gas [6, 7]. Therefore the initial values of the neutral particle and electron density, the heavy particle temperature and velocity at $z = 2$ mm are determined from the adiabatic calculation. The values for the densities are checked by comparing them to an extrapolation of the measured densities by the Thomson–Rayleigh measurements. For the electron temperature, the value obtained from an extrapolation of the measurement of T_e to $z = 2$ mm is used. Then the plasma parameters are calculated starting from $z = 2$ mm. The start of the shock transition for the neutral particles and ions for the standard condition is at approximately $z = 40$ mm. As discussed, a Mott–Smith solution was assumed after this position by which

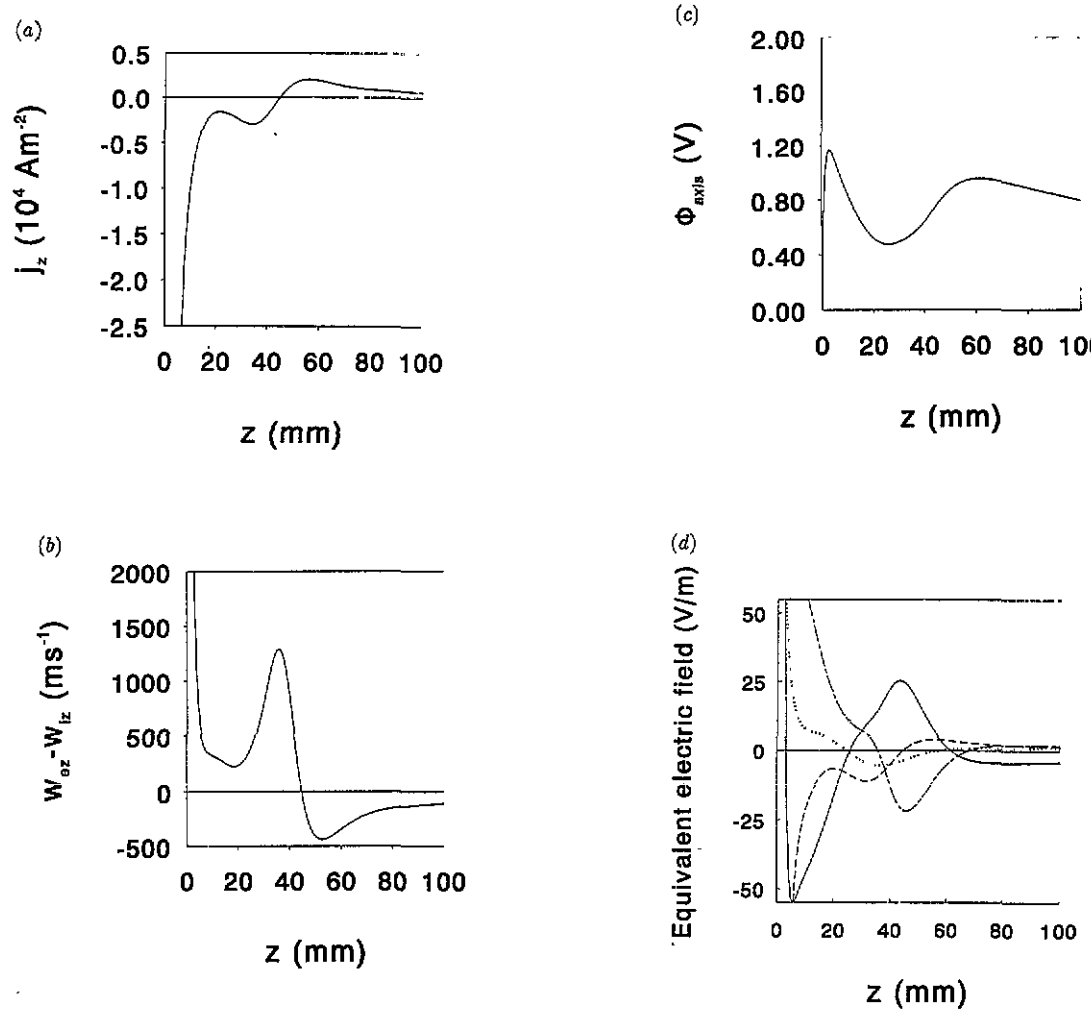

Figure 2. The results of the calculation of the electric properties on the axis for setting 1 of table 1: (*a*) the current density j_z, (*b*) the velocity difference $w_{ez} - w_{Iz}$, (*c*) the electric potential Φ_{axis} and (*d*) the different terms in the electron momentum balance expressed in an equivalent electric field. ——, E_z; – – –, ηj_z; — — —, $(en_e)^{-1}\partial p_e/\partial z$; . . . , $(\gamma_0 k_b/e)\partial T_e/\partial z$.

the electron energy balance was solved. However, the Mach numbers $M_{0,1}$ and M_1 in front of the shock are determined from the calculation [6]. The thickness of the ion and neutral particle shock is determined from these Mach numbers [36, 37]. Furthermore, the Mach numbers are used to determine the ion and neutral particle density and the heavy particle temperature in the shock fronts. The stability of the Runga–Kutta integration was checked by step dividing.

In figure 3 the results of the calculations for the electron and heavy particle temperature, the electron and neutral particle density and the heavy particle velocity are shown for the first 80 mm in the supersonic expansion and compared with the measurements taken with the setting of table 1. To illustrate the influence of current generation, the three-particle recombination and electron heat conduction, three different situations are considered.

The first calculation in figure 3 corresponds to an estimated value of the recombination energy $E_{rec,3} = 0.15 \times I_{ion}$ [7], the experimentally determined $K_{rec,3}$ [7], and the calculated current density and electric field from the two-dimensional model (see figure 2). The second calculation is identical to the first calculation except that no current density or electric field is included. Compared with the first calculation the electron heat conduction is included in calculation three.

As can be seen from figures 3(*a*)–(*c*), the influence of the different conditions on the neutral particle properties, i.e. the heavy particle temperature and velocity and the neutral particle density, is small. This again confirms that the neutral particles expand adiabatically to a good approximation [6, 7]. The agreement with the measurement of the neutral density is good even in the shock region. However, the Mach number as determined from the calculation was about a factor of two larger than the

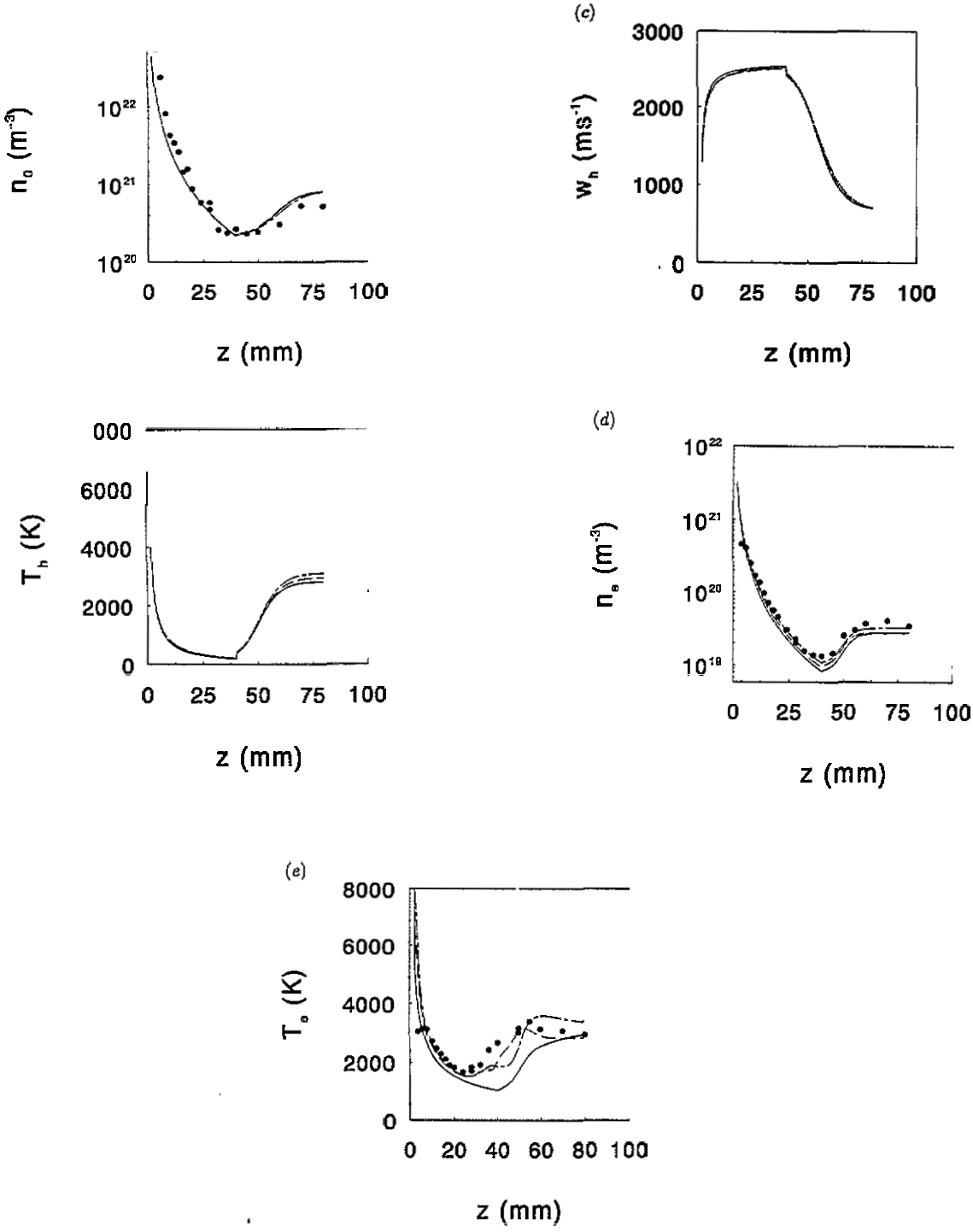

Figure 3. The calculated plasma parameters (*a*) the neutral particle density n_n, (*b*) the heavy particle temperature T_h, (*c*) the heavy particle velocity w_h, (*d*) the ion density n_i ($= n_e$) and (*e*) the electron temperature for three different situations explained in the text: (1) —— no electrical properties and no heat conduction included, (2) — — — identical to (1) except electrical properties included, (3) – – –, identical to (2) including the heat conduction.

calculated Mach number from the measured shock strength [6]. As follows from a comparison with the results of Meulenbroeks *et al* [39], the calculated temperatures of the heavy particles are too low. This is probably related to the fact that the temperatures measured by Meulenbroeks *et al* [39] reflect a large contribution of the ions since the only emission measured with the Fabry–Pérot interferometer in the expanding plasma jet originates from recombination, either two-particle or three-particle recombination. For instance, if

the ions gain energy in the electric field of the electrons, it is possible that this energy is dissipated by the ions which in turn heat the neutral particles. Note that a smaller Mach number does not influence the behaviour of the densities if the condition $M_p \gg 1$ remains fulfilled (see equations (17)–(27)). The small discontinuity in both the heavy particle temperature and velocity is due to the implementation of the Mott–Smith solution for the shock front at $z = 40$ mm.

The ion density in the expansion region is influenced in an indirect way. If the current density and recombination are absent the electron temperature decreases to a low value $T_e < 900$ K, which leads to a significant recombination because of the strong T_e dependence of $K_{rec,3}$ [7]. As can be seen from figure 3(*d*) the agreement with the measured electron density is good if the current density is included.

As can be seen in figure 3(*e*) the electron temperature depends strongly on the different conditions considered. From a comparison of the calculations it can be concluded that no electron temperature jump appears ahead of the density shock fronts if no current is present in the jet section. If the current density is included the electron temperature jump occurs at approximately the correct position. Furthermore, the presence of a current density and three-particle recombination heats the electron gas in the supersonic expansion region although the influence of the current density up to $z = 25$ mm is small. If heat conduction is included the structure in the electron temperature is smoothed out. The position of the electron temperature jump, however, is ruled by the current density. The influence of the electron heat conduction in the expansion is small. The agreement with the measurements of T_e is good. So to conclude this section, in contrast with the literature [15, 16, 40], in the present situation an explanation for the preheating of the electron gas is based on the effect of the presence of a current density and an electric field in combination with electron heat conduction.

5. Conclusions

An interesting observation is the fact that the electron temperature increases ahead of the density shock fronts [6]. In addition to the influence of the large electron heat conduction, this electron temperature jump is explained by the current density present in the expansion, which by Ohmic dissipation, heats the electron gas in front of the shock. The calculation of the electric properties of the expanding plasma show that the velocity difference between the ions and electrons, of the order of $500–1000\ m\ s^{-1}$, is never larger than at the exit of the cascaded arc. Just in front of the ion shock the velocity difference increases leading to the electron temperature jump. It is shown in these calculations that the current density is pressure induced. With the results of the two-dimensional calculations the plasma parameters are calculated in the one-dimensional model. The outcome of these calculations shows good agreement with the measured values of the electron and neutral particle density and the electron temperature.

Acknowledgments

We thank M J F van de Sande, H M M de Jong and A B M Hüsken for their skillful technical assistance. We also thank H J G Gielen for helpful discussions. The research of M C M van de Sanden has been made possible by a fellowship of The Royal Netherlands Academy of Arts and Sciences.

References

[1] Beulens J J, Buuron A J M and Schram D C 1991 *Surf. Coatings Technol.* **47** 401
[2] Buuron A J M, Beulens J J, van de Sande M J F, Schram D C and van der Laan J G 1991 *Fusion Technol.* **19** 2049
[3] Meeusen G J, Ershov-Pavlov E A, Meulenbroeks R F G van de Sanden M C M and Schram D C 1992 *J. Appl. Phys.* **71** 4156
[4] de Graaf M J, Severens R, Dahiya R P, van de Sanden M C M and Schram D C 1993 *Phys. Rev.* E 48 2098
[5] Ruyten W M and Keefer D 1992 *Appl. Phys. Lett.* **61** 880
[6] van de Sanden M C M, de Regt J M and Schram D C 1994 *Plasma Sources Sci. Technol.* **3** 501
[7] van de Sanden M C M, de Regt J M and Schram D C 1993 *Phys. Rev.* E **47** 2792
[8] Fraser R B, Robben F and Talbot L 1971 *Phys. Fluids* **14** 2317
[9] Kirchhoff R H and Talbot L 1971 *AIAA J.* **9** 1098
[10] Jenkins R C 1971 *AIAA J.* **9** 1383
[11] Poissant G and Dudeck M 1985 *J. Appl. Phys.* **58** 1772
[12] Christiansen W H 1967 *Phys. Fluids* **12** 2586
[13] Bogen P, Dippel K H, Hintz E and Siemsen F 1971 *Proc. ICPIG vol 10 (Oxford)*
[14] McNeill D H 1975 *Phys. Fluids* **18** 44
[15] Grewal M S and Talbot L 1963 *J. Fluid Mech.* **16** 573
[16] Jaffrin M Y and Probstein R P 1964 *Phys. Fluids* **10** 1658
[17] Imshennik V S 1962 *Sov. Phys.–JETP* **15** 167
[18] Nelson H F 1973 *Phys. Fluids* **16** 2132
[19] Vinõlo A R and Clarke J H 1973 *Phys. Fluids* **16** 1612
[20] Beulens J J, Milojevic D, Schram D C and Vallinga P M 1991 *Phys. Fluids* B **3** 2548
[21] Kroesen G M W, Schram D C and de Haas J C M 1990 *Plasma Chem. Plasma Proc.* **10** 531
[22] van de Sanden M C M 1991 PhD thesis University of Technology of Eindhoven, The Netherlands
[23] Braginskii S I 1965 *Reviews of Plasma Physics* ed M A Leontovich (New York: Plenum)
[24] Landau L and Liftshitz E 1989 *Fluid Mechanics* (London: Pergamon)
[25] Gielen H J G 1989 PhD thesis University of Technology of Eindhoven, The Netherlands
[26] Kroesen G M W, Schram D C, Timmermans C J and de Haas J C M 1990 *IEEE Trans. Plasma Sci.* **18** 985
[27] Frost L S 1961 *J. Appl. Phys.* **32** 2029
[28] Hamel B B and Willis D R 1966 *Phys. Fluids* **9** 829
[29] Chou Y S and Talbot L 1967 *AIAA J.* **5** 2166
[30] Goldfinch J 1971 *J. Plasma Phys.* **6** 153
[31] de Haas J C M 1986 PhD thesis University of Technology of Eindhoven, The Netherlands

[32] Owczarek J A 1964 *Fundamentals of Gas Dynamics* (Scranton: International Textbook)
[33] Gielen H J G and Schram D C 1990 *IEEE Trans. Plasma Sci.* **18** 127
[34] Young W S 1975 *Phys. Fluids* **18** 1421
[35] Mott–Smith H M 1951 *Phys. Rev.* **82** 885
[36] Muckenfuss C 1960 *Phys. Fluids* **3** 320
[37] Glansdorff P 1962 *Phys. Fluids* **5** 371
[38] Greenberg O W, Sen H K and Treve Y M 1960 *Phys. Fluids* **3** 379
[39] Meulenbroeks R F G, van der Heijden P A A, van de Sanden M C M and Schram D C 1994 *J. Appl. Phys.* **75** 2775
[40] Shafranov V D 1957 *Sov. Phys.–JETP* **5** 1183